*Korean J. Chem. Eng.*, 39(7), 1850-1862 (2022)
DOI: 10.1007/s11814-021-1056-1

pISSN: 0256-1115
eISSN: 1975-7220

# Removal of direct dyes by coagulation: Adaptability and mechanism related to the molecular structure

**Qunshan Wei*,†, Yanxia Zhang*, Kai Zhang*, Josphat Igadwa Mwasiagi**, Xiaoxiang Zhao*, Christopher W. K. Chow***, and Rui Tang***

*College of Environmental Science and Engineering, Donghua University, Shanghai 201620, China
**School of Engineering, Moi University, Box 3900-30100, Eldoret, Kenya
***Scarce Resources and Circular Economy (ScaRCE), UniSA STEM, University of South Australia, Mawson Lakes, SA 5095, Australia

(*Received 3 October 2021 • Revised 2 December 2021 • Accepted 29 December 2021*)

**Abstract**−The textile industry uses a variety of synthetic dyes for dyeing and discharges a large amount of colored wastewater. It is difficult to achieve good decolorization effect for textile wastewater by conventional biological treatment methods, because it contains various synthetic dyes with complex structures. At present, coagulation is an economical and effective treatment method. However, in dye removal by coagulation research, the adaptability and mechanisms of coagulation removal of many dyes are still unknown due to the wide variety of dyes in use. In this study, ferric chloride ($FeCl_3$), aluminum chloride ($AlCl_3$) and magnesium chloride ($MgCl_2$) were selected as coagulants, and direct orange 26 (DO), direct yellow 11 (DY) and direct black 19 (DB) were used as the dye samples to conduct a series of coagulation experiments; in order to understand the coagulation adaptability and mechanism for high removal efficiency of direct dyes. In this system without particles, the direct dyes were dissolved directly in pure water and maintained in molecular state. The results showed that 1) $AlCl_3$, $FeCl_3$ and $MgCl_2$ exhibited superior coagulation efficiency on the three dyes. Direct dyes which contain more amino functional groups are more easily removed by coagulation. 2) The influence of hydraulic conditions on the residual turbidity was more significant compared with the color removal. 3) Zeta potential increased with the increase of the coagulant dosage, but the colloidal particles did not re-stabilize. This proved that charge neutralization is not the dominant mechanism of coagulation. The FT-IR and XRD patterns indicated that the direct dyes were removed by the chemical combination of the -$SO_3H$ on the dye molecule and the hydrolysate of the coagulant.

Keywords: Inorganic Coagulant, Direct Dye, Coagulation Characteristics, Molecular Structure, Mechanism

## INTRODUCTION

Textile wastewater poses many challenges during treatment due to its complex composition, high level of pollutants, large discharge capacities and poor biodegradability [1,2]. The majority of chemical substances remaining in textile wastewater after the dyeing or printing processes are mainly dyes and/or pigments. Some of the dyes and pigments exhibit bio-toxicity and carcinogenicity characteristics and are difficult to degrade naturally. This leads to ecological imbalance of the polluted waters and poses a great threat to human health and other organisms. Nowadays, there are many treatment processes for printing and dyeing wastewater, such as adsorption [3], coagulation [4], combined coagulation and membrane filtration, advanced oxidation technology [5,6], and bio-treatment [7]. Zhao et al. [8] applied the synthesized self-assembled chitosan-based POSS-CNTs-CS nanocomposite to dye wastewater treatment to obtain excellent adsorption effect. Rehman et al. [9] prepared self-assembled hierarchical $Cu_xO@C_{18}H_{36}O_2$ nanoflakes and applied them to wastewater treatment, and found excellent adsorption capacity for RhB and superior Fenton-like catalytic efficiency and stability. Beluci et al. [10] improved the removal rate of reactive black 5 by combining coagulation and membrane filtration. At present, some nanocomposite materials have also been applied to the coagulation process. These nanocomposite coagulants have stable coagulation performance. Eslam et al. [11] prepared $Fe_2O_3$-$Mn_2O_3$ nanocomposites and applied them to the coagulation treatment of As (V). Li et al. [12] prepared a multi-core magnetic nano-polyaluminum silicate-iron-calcium composite (PSACF@FeNPs) and found that different (Al+Fe)/Ca ratios will affect the stability of the coagulant nanocomposite. Out of these common treatment options, coagulation has been widely applied to the treatment of textile wastewater due to its ease of operation, good efficiency and low cost [13,14].

Direct dyes are those dyes with water-soluble groups such as sulfonic acid group (-$SO_3H$) or carboxyl group (-COOH), and most of them are azo dyes. Adsorption is an effective method applied to the removal of direct dyes but comes with high treatment cost. Coagulation is the most economical and effective method used to remove disperse and reactive dyes, but few studies have been reported on its removal of direct dyes from dye effluents. Due to the differences in the structure and properties of dyes, specific experiments are needed for different direct dyes. In the coagulation liter-

†To whom correspondence should be addressed.
E-mail: qswei@dhu.edu.cn
Copyright by The Korean Institute of Chemical Engineers.

ature on direct dyes removal by coagulation, Shi et al. explored the removal performance of three different aluminum-based coagulants on direct dyes. The results showed that aluminum ion ($Al^{3+}$) exhibited excellent color removal of both direct blue 86 and direct black 19, while $AlCl_3$ had a better color removal efficiency on direct red 28 [15]. Aboelfetoh et al. used chitosan to aid the coagulation of graphene oxide, which improved its coagulation effect on direct brown 2 [16]. The electro-flocculation flotation process was applied to the removal of Direct Blue 71, and the color removal rate reached 99.4% [17]. There is also a lack of experimental data on different coagulants used for the study of coagulation treatment of direct dyes. Most of the existing data are mainly on the exploration of the influence of coagulant dosage and pH of solution on the coagulation effect; they lack comprehensive study of all other factors which can influence the coagulation process. The characteristics of the flocs formed after coagulation and the coagulation mechanism need to be further explored with in-depth research. The development of composite coagulants [18-21] and their use in coagulation treatment of printing and dyeing wastewater has received extensive attention and shown good application value. However, due to the lack of basic data, theoretical references and information on coagulation removal characteristics and mechanisms of many dyes, the development of composite coagulants is limited. Therefore, the prepared composite coagulants so far cannot achieve universal applicability.

Reports on the working of coagulation mechanism during the treatment of waste water indicates that the coagulation mechanism is not unified. The coagulation mechanism is mainly dependent on the type of coagulant and the type of dye [22]. Lu et al. believed that the mechanism of coagulation that removes microplastics and tetracycline is mainly sweep flocculation and adsorption [23]. Hailu et al. prepared a nanocluster-based coagulant whose coagulation mechanism for dyes was adsorption [24]. Yeap et al. reported that when a novel synthesized polyaluminum chloride-poly(3-acrylamido-isopropanol chloride) (PACl-PAMIPCl) an inorganic-organic hybrid polymer was used for the treatment of reactive blue dye wastewater, charge neutralization played a dominant role, while the disperse dye was mainly removed by adsorption bridging [25]. Yang et al. used a polyferric chloride-poly-epichlorohydrin-dimethylamine (PFC-ECH-DAM) composite flocculant to remove reactive blue dye, and found that charge neutralization was not the only dominant mechanism, but rather adsorption bridging effect of organic polymer components played an important role [26]. Li et al. found that the coagulation mechanism of magnesium salt was mainly through combined effect of sweep flocculation and charge neutralization, when he explored the effect of kaolin on removing reactive orange dye by magnesium hydroxide [27]. Bouyakoub et al. reported that the mechanism of $MnCl_2$ and $MgCl_2$ for the removal of reactive dye Levafix bright blue EBR from textile wastewater could best be described that the adsorption phenomenon was the basis for new precipitation, whereas the charge neutralization mechanism was the basis for the formation of aggregates [28]. Therefore, in view of the huge coagulant and dye combinations, the coagulation mechanism cannot be generalized, but needs to be analyzed in detail.

In previous studies, reactive dyes and disperse dyes were often used to prepare the dye test samples, whereas direct dyes were rarely investigated. In this study, three traditional inorganic coagulants, $AlCl_3$, $FeCl_3$ and $MgCl_2$, were selected. Based on the differences in dye structure, functional group and molecular weight, three representative direct dyes (direct orange 26 (DO), direct yellow 11 (DY) and direct black 19 (DB) were chosen to prepare the dye samples, so as to explore the coagulation effect and flocs characteristics under different coagulation conditions, and to study the binding mechanism of traditional inorganic coagulants with direct dyes. This study was expected to enrich and perfect the "industry and application database" of the coagulation process for the removal of dyes from textile wastewater, and provide a theoretical basis for the selection of appropriate coagulants and targeted coagulants.

## MATERIALS AND METHODS

### 1. Chemicals and Equipment

Aluminum chloride ($AlCl_3 \cdot 6H_2O$), ferric chloride ($FeCl_3 \cdot 6H_2O$), magnesium chloride ($MgCl_2 \cdot 6H_2O$), sodium hydroxide (NaOH), hydrochloric acid (HCl) were purchased from Sinopharm Chemical Reagents Co., Ltd., and all were analytical pure. Direct orange 26 (DO), direct yellow 11 (DY) and direct black 19 (DB) were purchased from Nanjing Dulai Biotechnology Co., Ltd., and their molecular formulas are shown in Table 1. The water used in the experiments was deionized water.

The equipment used in this research work included: Jar test apparatus (ZR4-6, Zhongrun Water Industry Technology Development Co., Ltd., China), pH meter (FE28, Mettler Toledo, Switzerland), Electronic balance (AL204, Mettler Toledo, Switzerland), Drying box (101-00B, Wei Heng Machinery, China), Turbidity meter (WZS-186, Lei Ci, China), UV-Vis spectrophotometer (Specord 200 Plus, Analytikjena, Germany), Nano particle size and zeta potential meter (90 Pals, Brook Haven, USA), Fourier transform infrared spectroscopy (FT-IR) meter (Tensor27, Bruker, Germany), X-ray diffractometer (D/ MAX-2550VB +/PC, Rigaku, Japan), Centrifuge (Himac CR 22GII, Hitachi, Japan), Fluorescent microscopy (Nikon 80i, Japan).

### 2. Experimental

2-1. Wastewater Sample and Coagulant

Simulated dyeing wastewater with a concentration of 50 mg/L was used for the experiments. DO, DY, and DB were, respectively, weighed and added into deionized water. After full dissolution, 5,000 mg/L dye stock solution was prepared and then diluted to 50 mg/L (the dye concentration used in this experiment). The concentrations of $AlCl_3$, $FeCl_3$ and $MgCl_2$ were 1 mol/L, 1 mol/L, and 4 mol/L, respectively.

2-2. Beaker Testing

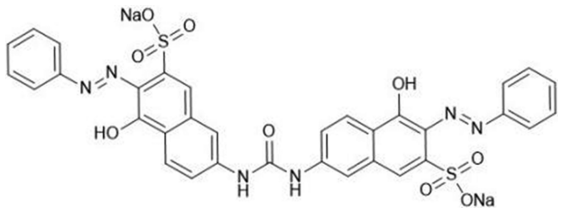
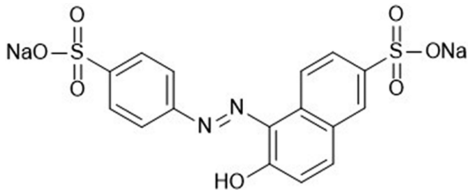
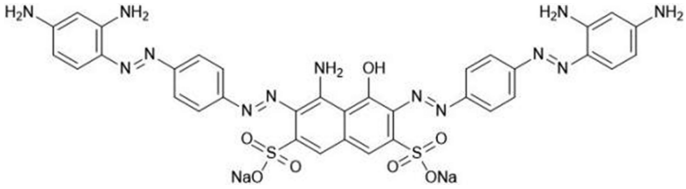
Standard beaker tests were carried out at room temperature. The coagulation procedure involved mixing (150 r/min, 1 min), rapid stirring (300 r/min, 1 min), slow stirring (50 r/min, 15 min) and settling (30 min). The supernatant at 3 cm below the liquid level was taken for the determination of relevant analysis after the end of the coagulation procedure. All measurements were carried out five times to ensure a high level of accuracy.

### 3. Analysis

3-1. Basic Coagulation Process Assessment

Different concentrations of coagulant were added to the simu-

**Table 1. Direct dyes**

| Name | Type | Structure formula | Molecular weight | $\lambda_{max}$ |
|---|---|---|---|---|
| DO | Azo |  | 756.67 | 492 |
| DY | Azo |  | 452.67 | 415 |
| DB | Azo |  | 839.77 | 670 |

DO: direct orange 26; DY: direct yellow 11; DB: direct black 19

lated dyeing wastewater. After the coagulation process, the supernatant was taken to determine the turbidity and Zeta potential. Turbidity and Zeta potential were measured using a turbidity meter and a Zeta potential meter, respectively. The supernatants used for absorbance measurements were filtered by a 0.45 μm filter membrane and analyzed using a UV-Vis spectrophotometer (1 cm quartz cell for UV measurement). The initial pH of the simulated dyeing wastewater was adjusted and the coagulation experiment was carried out under the optimal concentration of coagulant. After the coagulation process, the supernatant was filtered by a filter membrane of 0.45 μm and the absorbance (absorbance was measured at the $\lambda_{max}$ of the dye) was determined.

3-2. Effect of Different Hydraulic Conditions on Coagulation Effect

First, the rapid mixing time was set at 10, 30, 60 and 120 s, respectively, and the remaining procedures were consistent with the coagulation procedures in section 2.2.2. Then the coagulation experiment was carried out under the condition of optimum coagulant dosage. After the coagulation process, the turbidity and absorbance were measured.

During this test the stirring speeds used were 30, 40, 50, 60, 80, and 100 r/min, and the remaining procedures were also consistent with the coagulation procedures in section 2.2.2. The coagulation experiments were carried out under the condition of optimum coagulant dosage. After the coagulation process, the turbidity and absorbance were determined.

3-3. Floc Properties

Flocs were captured by a microscope with image capturing function, and the floc edge perimeter and projected area were analyzed by Image J software to calculate the floc particle size and two-dimensional fractal dimension $D_f$ [29].

The particle size of individual floc can be expressed by the diameter of a circle equal to the projected area of the floc. The average particle size (dp) of a single floc is calculated by using Eq. (1):

$$dp = 2\sqrt{\frac{A}{\pi}} \quad (1)$$

where, A ($\mu m^2$) is the projection area of a single floc.

The fractal dimension ($D_f$) can be calculated by Eq. (2) [30,31]:

$$A \propto P^{Df} \quad (2)$$

where, A ($\mu m^2$) is the projection area of floc; P (μm) is the projection circumference of floc.

3-4. The Effect of Changing the Order of Adding Coagulant

Under the optimal concentration of coagulant and the optimal initial pH of simulated dye wastewater, coagulant was added to the deionized water for hydrolysis before coagulation. Dye was added at the beginning of rapid stirring process, and the absorbance of the supernatant was determined after coagulation process.

3-5. Sediment Characterization

The flocs were characterized by FT-IR and XRD after centrifugation and drying.

## RESULTS AND DISCUSSION

### 1. Basic Coagulation Characteristics

1-1. Effect of Coagulant Dosage on Coagulation Performance

Coagulation experiments were conducted to treat direct dye waste water using three coagulants ($AlCl_3$, $FeCl_3$ and $MgCl_2$). The coagulant dosage ranges were determined as follows: $AlCl_3$ and $FeCl_3$: 0-0.3 mmol/L and $MgCl_2$: 0-6 mmol/L. This was in the same range as per results reported by other researchers [32]. Results of the investigation of residual turbidity and turbidity are given in Fig. 1.

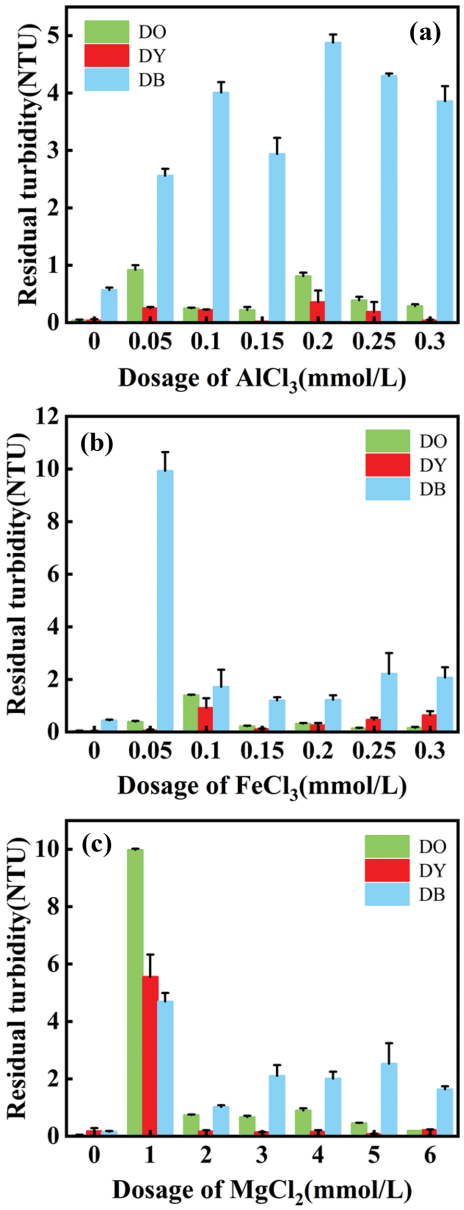



Fig. 1. Effect of coagulant dosage on residual turbidity of three dyes: (a) dyes treated with $AlCl_3$, (b) dyes treated with $FeCl_3$ and (c) dyes treated with $MgCl_2$. DO: direct orange 26; DY: direct yellow 11; DB: direct black 19.

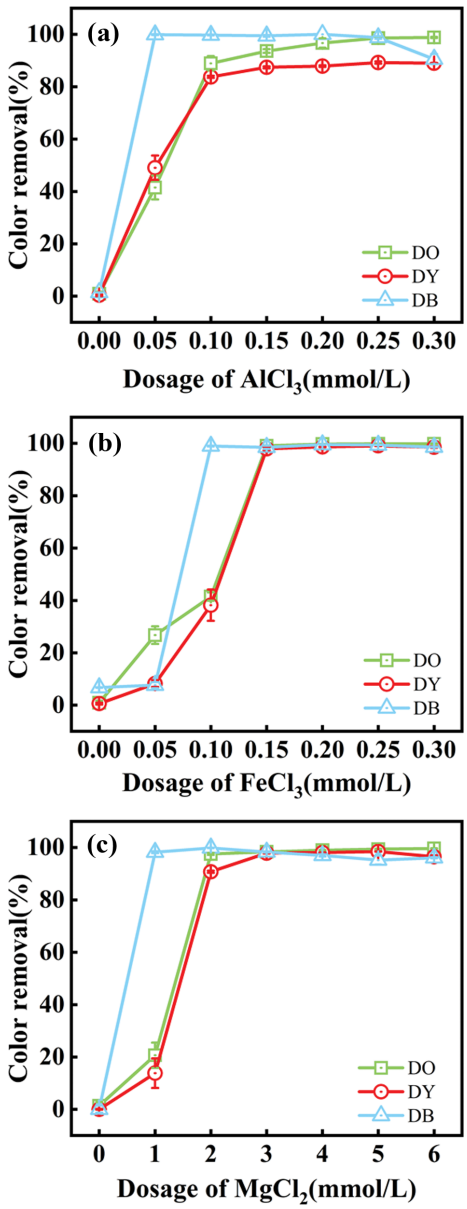



Fig. 2. Effect of coagulant dosage on the color removal: (a) dyes treated with $AlCl_3$, (b) dyes treated with $FeCl_3$ and (c) dyes treated with $MgCl_2$.

The influence of coagulant dosage on the residual turbidity as shown in Fig. 1, indicated that in a certain dosage range, the residual turbidity of the three direct dyes treated with different coagulants showed a trend of first increasing, then decreasing and finally increasing with the increase of coagulant dosage. At low coagulant dosage addition, the charge neutralization resulted in the destabilization of colloidal particles. However, due to low efficiency, flocs with good structures failed to form, resulting in higher residual turbidity. With the increase of the dosage of coagulant, the coagulant played a good role in reducing turbidity. Therefore, when DO, DY and DB had low residual turbidity, the optimal doses of $AlCl_3$ were 0.15, 0.15 and 0.05 mmol/L respectively. The optimal doses of $FeCl_3$ on the other hand, were 0.15, 0.15 and 0.15 mmol/L respectively, whereas the optimal doses of $MgCl_2$ were 2, 3 and 2 mmol/L respectively.

According to the linear relationship between dye concentration and absorbance value at $\lambda_{max}$, the percentage color removal R (%) by coagulation was calculated by Eq. (3):

$$R = \frac{A_0 - A}{A_0} \times 100\% \quad (3)$$

where, $A_0$ and A are absorbance values of the original dye solution measured at $\lambda_{max}$ of the corresponding dye. The supernatant sample was filtered by 0.45 μm membrane.

The effect of coagulant dosage on dye color removal is shown

in Fig. 2. In a certain dosage range, the dye color removal increased with the increase of the coagulant dosage. The color removal reached a plateau after the optimal dose was reached. To obtain the best color removal, the optimal coagulation dosage of $AlCl_3$ for DO, DY and DB was 0.15, 0.15 and 0.05 mmol/L, respectively, and the color removal of the three dyes was 93.0%, 87.4% and 99.8%, respectively. The optimal coagulant dosage of $FeCl_3$ for DO, DY and DB was 0.15, 0.15 and 0.10 mmol/L, respectively. The optimal coagulant dosage of $MgCl_2$ for DO, DY and DB was 2, 3 and 2 mmol/L, respectively.

As shown in both Fig. 2 and Fig. 1, the dosage of coagulant with the best color removal can also produce lower residual turbidity. Therefore, the dosage of coagulant with the best color removal was determined to be the optimal dosage of the coagulant.

Previous studies [33] have shown that if charge neutralization is the dominant coagulation mechanism, the colloid in the system will be re-stabilized because of the high positive charge, and the coagulation effect will become worse with the increase of the amount of coagulant. In this study, there was no phenomenon that showed that the coagulant efficiency became worse with increase in dosage of the coagulant. These results are contradicted by other researchers [34]. Therefore, we infer that based on the results obtained in this research works, dominant coagulation mechanism of the selected coagulants for direct dyes was not electric and neutralization. Although an excessive amount of coagulant will not affect the color removal of the direct dyes, it will affect the formation of flocs and cause the residual turbidity of the wastewater to become larger, which in turn affects the subsequent treatment of the wastewater. Therefore, it is necessary to choose the appropriate amount of coagulant to achieve the optimum effect of color removal and residual turbidity, while reducing the cost of dosing.

$AlCl_3$, $FeCl_3$ and $MgCl_2$ had good color removal efficiency on three direct dyes at low dosages. In contrast, the color of DB was removed more easily than that of DO and DY. In their study of the effect of dye structure on the rate of color removal by coagulation, McYotto et al. [32] found that disperse dyes and other dyes which have acidic functional groups (such as $-SO_3Na$, -NH-) can coordinate with metal ions to form relatively hydrophobic complexes, which can then be more easily removed by coagulation. In this study, DB was easier to remove by coagulation than the other two dyes because it had more amino functional groups. At the same time, DB had a larger molecular weight and longer molecular chain structure than the other two dyes, which also helped DB to be removed more easily by coagulation. DY, which had no amino functional groups in its molecular structure and had the smallest molecular weight, had the lowest color removal efficiency.

1-2. Effect of Initial pH of Simulated Wastewater on Color Removal Efficiency

NaOH and HCl were used to adjust the initial pH value of the dye to investigate the influence of pH on the color removal efficiency under the optimal dosage of coagulant. The results are shown in Fig. 3. The coagulation effect was different under different pH condi-

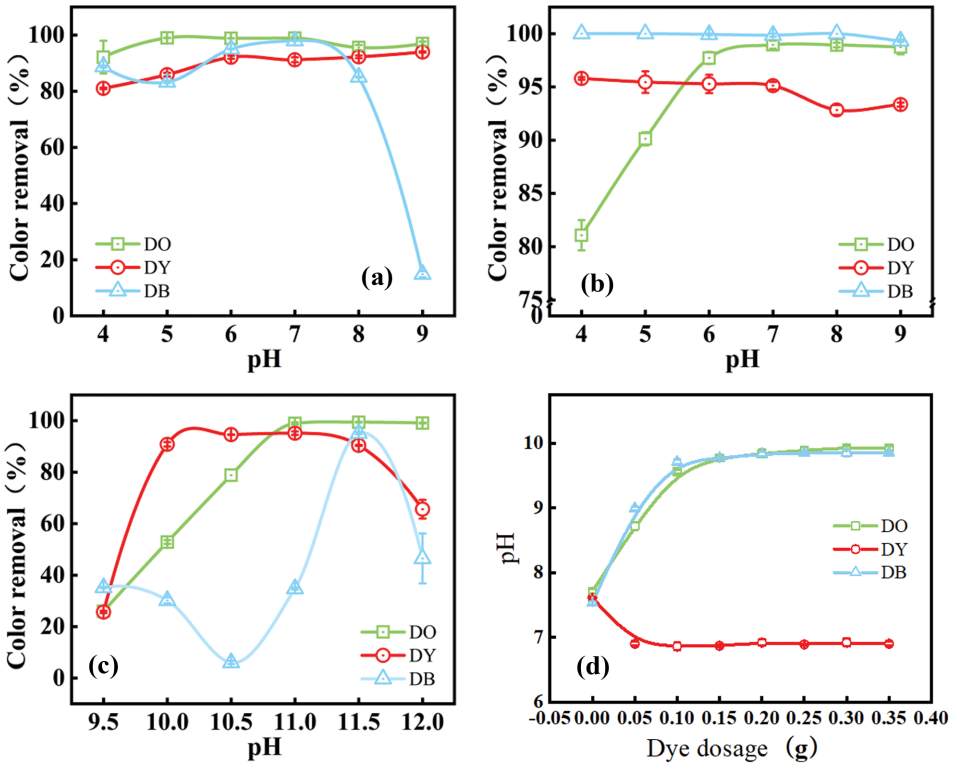



**Fig. 3. Effect of initial pH of dye on the color removal efficiency: (a) dyes treated with $AlCl_3$; (b) dyes treated with $FeCl_3$; (c) dyes treated with $MgCl_2$; (d) Mass titration curve of dye, titration solution is 0.05 mol/L NaCl. [1]Optimum dosage of each experimental group: $AlCl_3$-DO, $AlCl_3$-DY, $FeCl_3$-DO, $FeCl_3$-DY: 0.15 mmol/L; $AlCl_3$-DB: 0.05 mmol/L; $FeCl_3$-DB: 0.10 mmol/L; $MgCl_2$-DO, $MgCl_2$-DB: 2 mmol/L; $MgCl_2$-DY: 3 mmol/L. [2]$MgCl_2$ coagulates under alkaline conditions, so the pH range is set to 9.5-12.**

tions, and different pH ranges were suitable for the removal of dyes by coagulants.

It can be seen from Fig. 3(a) and 3(b) that in the pH range of 6-9, $AlCl_3$ had a good coagulation effect on DY, and the color removal was around 92%; $FeCl_3$ had a good coagulation effect on DO and DB and the removal of the dyes was about 98%, 99%, respectively. The color removal of $AlCl_3$ on DB and DY was about 96% and 95% respectively when the pH value was in the range of 6-7. The color removal of $AlCl_3$ on DO reached 98% in the range of pH 5-7. The negatively charged colloidal particles and the mononuclear or poly-nuclear hydroxyl ions formed by the hydrolysis of the coagulant functioned better under suitable pH conditions. Therefore, the pH value of 6-7 was the common range for $AlCl_3$ and $FeCl_3$ to remove direct dyes. Magnesium salt exerted better coagulation performance under high pH conditions [35]. Fig. 3(c) shows that $MgCl_2$ had the best coagulation effect on DO, DY, and DB when the pH was 11-12, 10.5-11 and 11.5, respectively, and the color removal reached about 99%, 95%, and 95%, respectively. Controlling the pH of coagulation of wastewater during the process enhanced the effectiveness of the coagulant and improved the overall coagulation efficiency. In the subsequent experiments, the pH of dye simulated wastewater was adjusted to the optimal range.

The point of zero charge (PZC) of three dyes was measured by mass titration. The PZC of DO, DY, and DB were 9.94±0.04, 6.95±0.03, and 9.85±0.02, respectively. When the pH was lower than the PZC of the substance, the surface of the substance was positively charged; otherwise, it was negatively charged. From Fig. 3abc, we can know the pH range when the coagulation effect was the best. For $AlCl_3$ and $FeCl_3$, the optimal pH for coagulation was lower than the PZC of dyes. At this time, the surface of the dye was positively charged, whereas the coagulant was positively charged after hydrolysis. Thus, the electrostatic adsorption effect of the two was weakened, which further confirmed that electric neutralization was not the dominant mechanism of coagulation; chemical bonding played an important role in the removal of dyes. For $MgCl_2$, the optimal pH for coagulation was higher than the PZC of the dye. The surface of the dye molecule was negatively charged, whereas $MgCl_2$ was positively charged after hydrolysis.

**2. Influence of Hydraulic Conditions on Coagulation Performance**

2-1. The Effect of Rapid Mixing Time

The influence of rapid mixing time on the residual turbidity of dye simulated wastewater after coagulation is shown in Fig. 4. Floc characteristics such as floc sedimentation can be significantly affected by the rapid mixing time, thus affecting the solid-liquid separation process [36].

The results showed that the effect of rapid mixing time on the residual turbidity was obvious, and there was a significant difference in the residual turbidity under different rapid mixing time. With the increase of rapid mixing time, the residual turbidity first decreased and then increased subsequently. For direct dyes, different coagulants had different optimal rapid mixing times. For example, for DO, the best rapid mixing time of $AlCl_3$ and $FeCl_3$ was 60 s, while that of $MgCl_2$ was 30 s.

The effect of rapid mixing time on color removal efficiency is shown in Fig. 5. The results show that the color removal efficiency

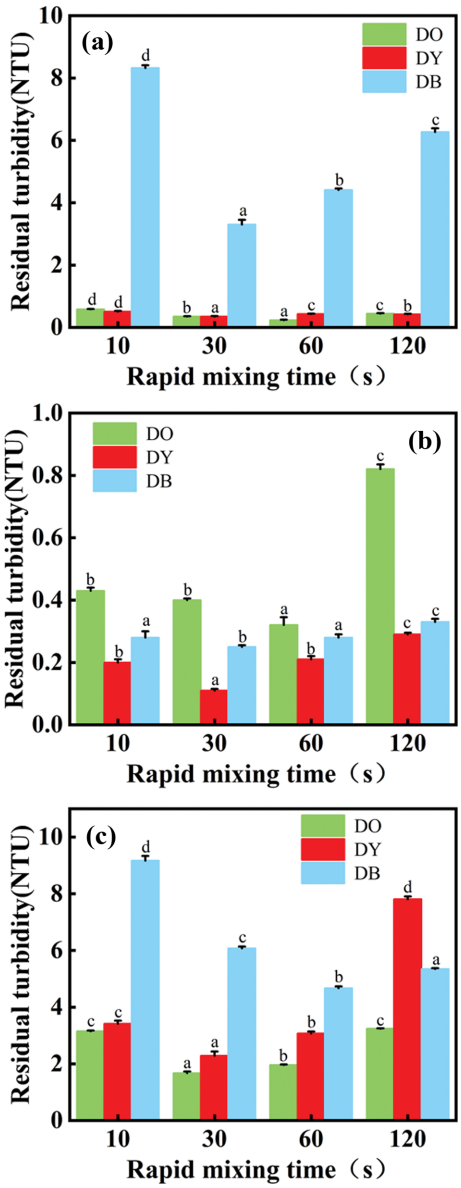



**Fig. 4. Effect of rapid mixing time on residual turbidity: (a) dyes treated with $AlCl_3$; (b) dyes treated with $FeCl_3$; (c) dyes treated with $MgCl_2$. [1]Optimum dosage of each experimental group: $AlCl_3$-DO, $AlCl_3$-DY, $FeCl_3$-DO, $FeCl_3$-DY: 0.15 mmol/L; $AlCl_3$-DB: 0.05 mmol/L; $FeCl_3$-DB: 0.10 mmol/L; $MgCl_2$-DO, $MgCl_2$-DB: 2 mmol/L; $MgCl_2$-DY: 3 mmol/L. [2]The letters (a, b, c, d) in the same column of the same coagulant value indicate significant differences compared to other treatment at $p<0.05$ according to Duncan's multiple range test.**

of $AlCl_3$-DY, $FeCl_3$-DY, $MgCl_2$-DY and $MgCl_2$-DB groups was significantly different under different rapid mixing times. The color removal increased first and then decreased subsequently with the prolongation of rapid mixing time. For the other experimental sets, the color removal under different rapid mixing time had no significant difference. Comparing Fig. 5 with Fig. 4, it could be deduced that under optimum conditions of the rapid mixing time, the highest color removal corresponded to the lowest residual turbidity.

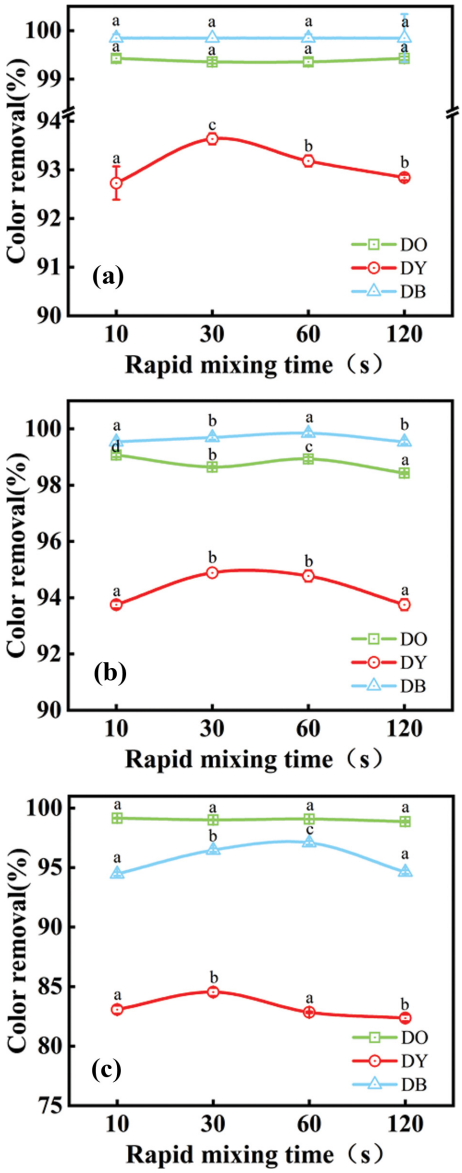



**Fig. 5. Effect of rapid mixing time on color removal efficiency: (a) dyes treated with $AlCl_3$; (b) dyes treated with $FeCl_3$; (c) dyes treated with $MgCl_2$. [1]Optimum dosage of each experimental group: $AlCl_3$-DO, $AlCl_3$-DY, $FeCl_3$-DO, $FeCl_3$-DY: 0.15 mmol/L; $AlCl_3$-DB: 0.05 mmol/L; $FeCl_3$-DB: 0.10 mmol/L; $MgCl_2$-DO, $MgCl_2$-DB: 2 mmol/L; $MgCl_2$-DY: 3 mmol/L. [2]The letters (a, b, c, d) in the same column of the same coagulant value indicate significant differences compared to other treatment at $p<0.05$ according to Duncan's multiple range test.**

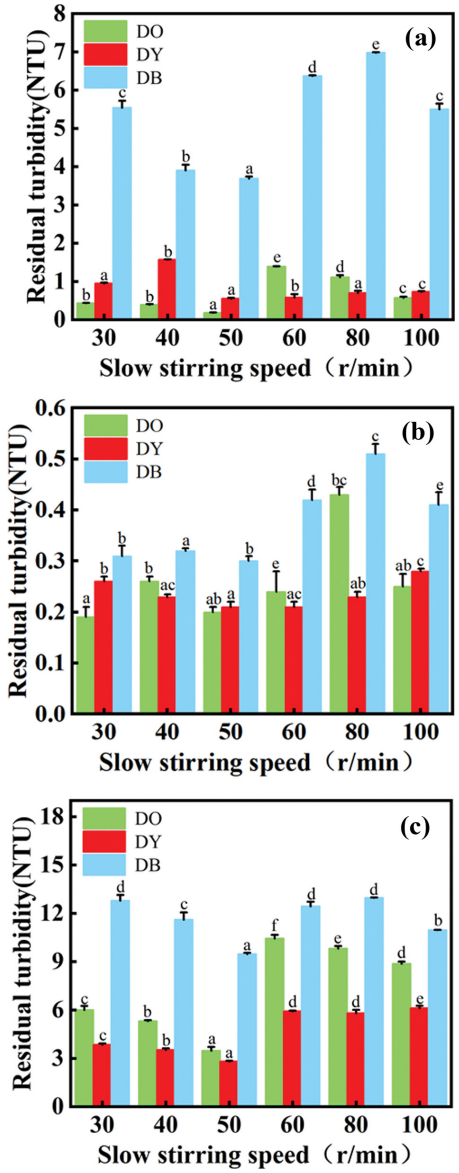



**Fig. 6. Effect of slow stirring speed on residual turbidity: (a) dyes treated with $AlCl_3$; (b) dyes treated with $FeCl_3$; (c) dyes treated with $MgCl_2$. The Optimum dosage of each experimental group was as follows: $AlCl_3$-DO, $AlCl_3$-DY, FeCl3-DO, and $FeCl_3$-DY: 0.15 mmol/L; $AlCl_3$-DB: 0.05 mmol/L; $FeCl_3$-DB: 0.10 mmol/L; $MgCl_2$-DO and $MgCl_2$-DB: 2 mmol/L; $MgCl_2$-DY: 3 mmol/L. The letters (a, b, c, d) in the same column of the same coagulant value indicate significant differences compared to other treatment at $p<0.05$ according to Duncan's multiple range test.**

2-2. The Effect of Slow Stirring Speed

The effect of slow stirring speed on residual turbidity was carried out and the results are given in Fig. 6. Slow stirring during coagulation is a process by which fine particles effectively collide, aggregate and grow larger. If the slow stirring speed is too slow, the fine particles formed during the rapid mixing process cannot effectively collide and grow. On the other hand, if the slow stirring speed is too fast, it may break the formed flocs. Only at a suitable stirring speed can flocs with good structure be formed, good solid-liquid separation achieved and the best coagulation effect produced. As shown in Fig. 6, the slow stirring speed had a significant effect on the residual turbidity. The residual turbidity decreased first, then increased and then decreased subsequently again with the increase of slow stirring speed. The lowest residual turbidity was obtained when the slow stirring speed was 50 r/min.

The color removal efficiency under different slow stirring speed is shown in Fig. 7.

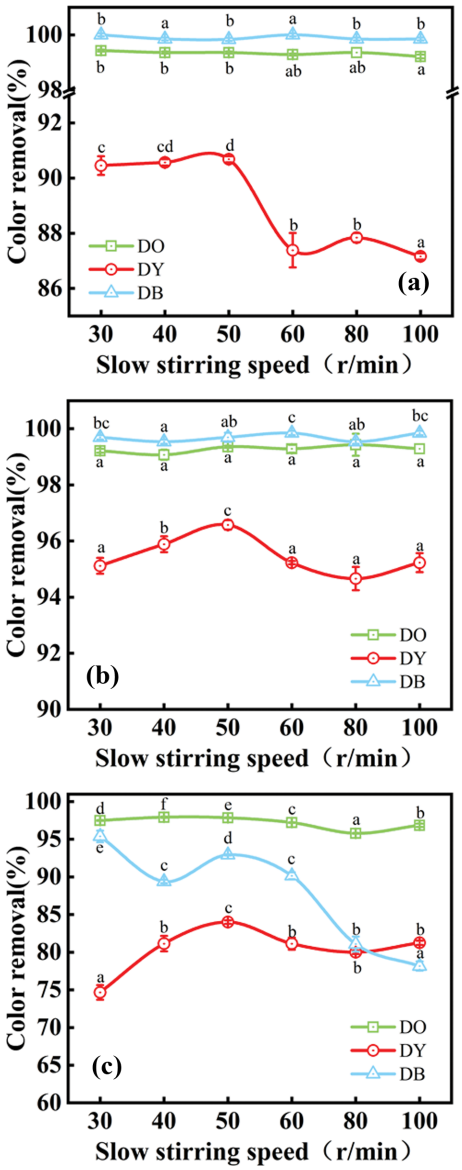



**Fig. 7. Effect of slow stirring speed on color removal efficiency: (a) dyes treated with $AlCl_3$; (b) dyes treated with $FeCl_3$; (c) dyes treated with $MgCl_2$. The Optimum dosage of each experimental group (Fig. 7) was as follows: $AlCl_3$-DO, $AlCl_3$-DY, $FeCl_3$-DO and $FeCl_3$-DY: 0.15 mmol/L; $AlCl_3$-DB: 0.05 mmol/L; $FeCl_3$-DB: 0.10 mmol/L; $MgCl_2$-DO and $MgCl_2$-DB: 2 mmol/L; $MgCl_2$-DY: 3 mmol/L. The letters (a, b, c, d) in the same column of the same coagulant value indicate significant differences compared to other treatment at $p<0.05$ according to Duncan's multiple range test.**

The results show that the color removal efficiency of $AlCl_3$-DY, $FeCl_3$-DY, $MgCl_2$-DY and $MgCl_2$-DB groups was significantly different under different slow stirring speeds. The highest color removal was achieved when the slow stirring speed was 50 r/min (this speed produced lower residual turbidity). For the other experimental groups, there was no significant change in color removal when the slow stirring speed was changed. This was the same as the effect of rapid mixing time on color removal efficiency.

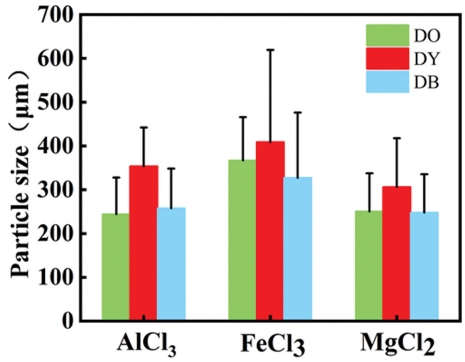



**Fig. 8. Particle size of flocs in different coagulation groups. The optimum dosage of each experimental group for the results in Fig. 8 was as follows: $AlCl_3$-DO, $AlCl_3$-DY, $FeCl_3$-DO and $FeCl_3$-DY: 0.15 mmol/L; $AlCl_3$-DB: 0.05 mmol/L; $FeCl_3$-DB: 0.10 mmol/L; $MgCl_2$-DO and $MgCl_2$-DB: 2 mmol/L; $MgCl_2$-DY: 3 mmol/L. Both $AlCl_3$ and $FeCl_3$ used a pH range of 6-7. For DO, DY and DB, the pH values were 11.5, 11, and 11.5, respectively.**

## 3. Characteristics of Flocs

### 3-1. Particle Size

The characteristics of flocs after different coagulants interacted with the direct dyes were analyzed by monitoring the particle size of flocs after coagulation. Under the best coagulation conditions, the supernatant floc size after coagulation is shown in Fig. 8.

For DO, DY, and DB, when $FeCl_3$ was used as a coagulant the particle size of flocs was larger than that of $AlCl_3$ and $MgCl_2$ as coagulants; the particle size was 366.8, 408.8 and 327.5 μm, respectively.

The particle size of the flocs produced by DY was larger than that of the other two dyes. The characteristics of flocs formed after coagulation were closely related to the types of coagulants and the properties of dyes. When $FeCl_3$ and $MgCl_2$ were used as coagulants, respectively, we found that the relationship of the particle size of the flocs produced by the three dyes was DY>DO>DB. The molecular weights of DY, DO, and DB were 452.37, 756.67, and 839.77, respectively. Therefore, it was inferred that there was a certain negative correlation between the particle size of the flocs produced by the dye and its molecular weight.

### 3-2. Fractal Features

Before the end of the slow mixing stage, samples were collected from the coagulated floc and placed on a glass slide and the image was recorded using a microscope (see Fig. 9).

Image J software was used to process the image, and the resultant fractal dimension calculation results are shown in Table 2.

According to Eq. (3), logA and logP would be linearly fitted. $R^2$ represents the correlation coefficient in Table 2. It can be seen from Table 2 that under the optimal coagulant dosage conditions, the correlation coefficients ($R^2$) of all flocs are in the range of 0.8883-0.9481. It shows that there was a good correlation between logA and logP. Generally, the floc has fractal characteristics when the fractal dimension is between 1.2 and 1.8 [37]. Except for the $AlCl_3$-DO group, the flocs $D_f$ produced in the other experimental groups were all within this range. It had obvious fractal characteristics.

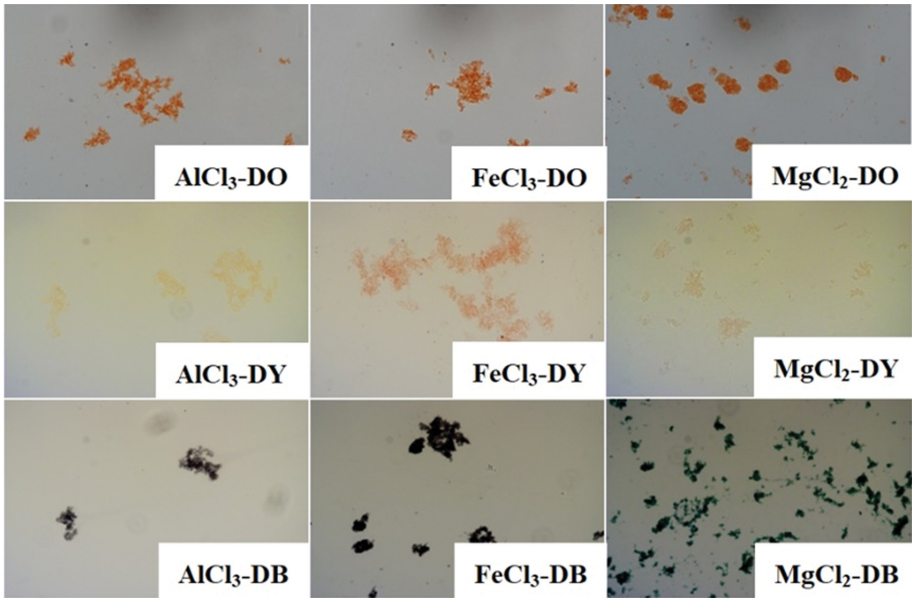



**Fig. 9. Floc images of different coagulation groups under optimal coagulation conditions. [1]Optimum dosage of each experimental group: $AlCl_3$-DO, $AlCl_3$-DY, $FeCl_3$-DO and $FeCl_3$-DY: 0.15 mmol/L; $AlCl_3$-DB: 0.05 mmol/L; $FeCl_3$-DB: 0.10 mmol/L; $MgCl_2$-DO and $MgCl_2$-DB: 2 mmol/L; $MgCl_2$-DY: 3 mmol/L. [2]Both $AlCl_3$ and $FeCl_3$ used a pH range of 6-7. For DO, DY and DB the pH values were 11.5, 11, and11.5 respectively.**

**Table 2. Two dimensional fractal dimensions under optimal coagulation conditions**

| | DO | | DY | | DB | |
|---|---|---|---|---|---|---|
| | $D_f$ | $R^2$ | $D_f$ | $R^2$ | $D_f$ | $R^2$ |
| $AlCl_3$ | 0.9951 | 0.9026 | 1.476 | 0.8976 | 1.4004 | 0.9289 |
| $FeCl_3$ | 1.3080 | 0.8883 | 1.6353 | 0.9481 | 1.3844 | 0.9125 |
| $MgCl_2$ | 1.4264 | 0.9189 | 1.3093 | 0.9322 | 1.2851 | 0.9173 |

Studies [38] showed that the larger the $D_f$ value of the floc had a dense structure, the fewer branches and the better the settlement performance was. On the other hand, the smaller the $D_f$ the looser the floc structure was and the more the branches were. Combining Fig. 9 and Table 2, it can be seen that in this experiment, the fractal dimension of flocs of the same dye after coagulation with different coagulants basically conformed with this conclusion: the larger the fractal dimension, the denser the floc structure and the fewer branches. For the three different dyes, the experimental combinations with the largest fractal dimension were $MgCl_2$-DO, $FeCl_3$-DY, $AlCl_3$-DB.

## 4. Analysis of Coagulation Mechanism

### 4-1. Zeta Potential

Under the action of different coagulants, the Zeta potentials of the three dye wastewaters at different coagulant dosages are shown in Fig. 10. The average Zeta potentials of the initial solutions of DO, DY, and DB were −25.51, −21.12 and −34.25 mv, respectively. As the dosage of coagulant increased, the Zeta potential of all the three dye solutions constantly increased. As shown in Fig. 2, as the amount of coagulant increased the color removal of dyes showed an upward increment trend. Particle re-stabilization did not occur within the investigated dosage range. According to the analysis of the existing data, the positively charged ions such as $Al^{3+}$ and $Fe^{3+}$ were generated by the hydrolysis of the coagulant in the water. These ions made the colloidal particles more attractive than the repulsive force through the action of charge neutralization and compression of the electric double layer, and the colloid began to destabilize causing the system to agglomerate rapidly [39]. At the same time, it was found that the Zeta potential was not close to 0 mv at the optimal coagulation dosage, indicating that the strongest electrostatic adsorption capacity was not required to produce the best coagulation effect. The best coagulation effect required electric neutralization and other coagulation mechanisms to work together.

The experimental results showed that when $FeCl_3$ was used as a coagulant and the dosage was 0.2 mmol/L, the zeta potential of the three dyes changed from negative to positive. When the dosage was 0.3 mmol/L, the Zeta potentials of DO, DY and DB reached 14.19, 17.36, and 11.76 mv, respectively. However, the coagulation effect did not deteriorate and there was no phenomenon of re-stabilization of particles. At this time, the electrostatic repulsion was smaller than other floc-forming forces, which further indicated that there were other mechanisms that played an important role in enhancing the coagulation effect. According to the study of Bouyakoub et al., the charge neutralization mechanism was the basis of the formation of aggregates when the selected inorganic coagulant removed direct dyes [28].

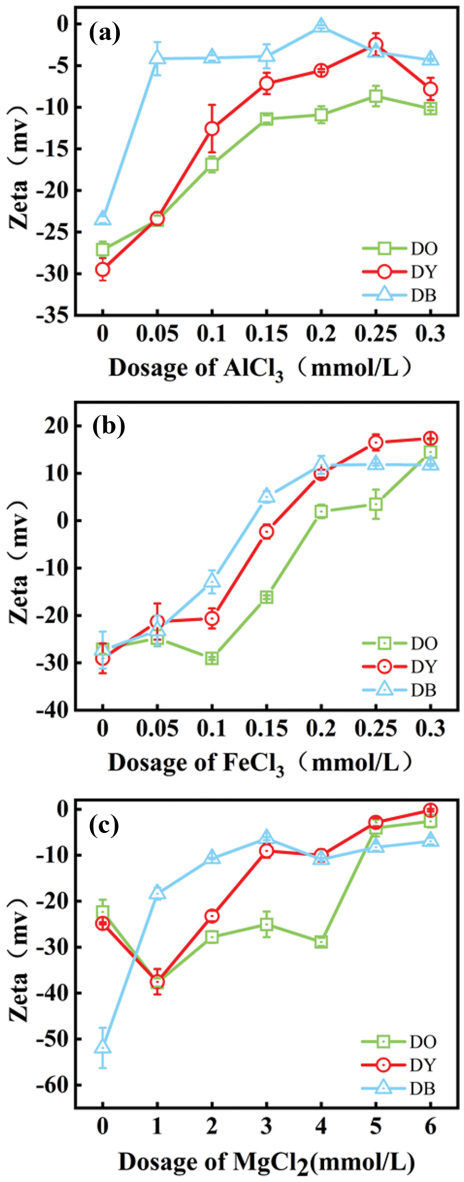



**Fig. 10. Variation of Zeta potential at different coagulant dosage: (a) dyes treated with $AlCl_3$; (b) dyes treated with $FeCl_3$; (c) dyes treated with $MgCl_2$.**

4-2. FT-IR and XRD

By investigating the absorption peaks of the FT-IR spectrum of 4,000-400 $cm^{-1}$, the changes in the molecular structure and chemical bonds of the flocs formed after dyes interacted with different coagulants were studied. The results are shown in Fig. 11(a), 11(b) and 11(c). The broad absorption peak at 3,200-3,650 $cm^{-1}$ was caused by the -OH in the dye structure and the -OH stretching vibration of the solid adsorbing or binding water molecules. The peak at about 1,600 $cm^{-1}$ was due to the bending vibration of bound water, which was caused by the deformation frequency of (H-O-H) [40, 41]. The absorption peak near 1,040 $cm^{-1}$ was attributable to the stretching vibrations of Fe-OH-Fe, Al-OH-Al and Mg-OH-Mg, and was also caused by the M-OH bending vibration on the molecular surface [42]. The absorption peak around 1,136 $cm^{-1}$ was caused by the stretching vibration of the $-SO_3H$ in the dye molecule. When the direct dyes reacted with the coagulants, the FT-IR spectrum showed that the absorption peak disappeared or weakened, which indicated that the coagulants reacted with the $-SO_3H$ in the dye molecule.

When $AlCl_3$ and $FeCl_3$ were used as coagulants, the absorption peaks of Al-O and Fe-O appeared near 480 $cm^{-1}$ (the peak appeared at 540 $cm^{-1}$ when the dye was DY). When $MgCl_2$ was used as a coagulant, all three direct dyes had very sharp peaks at 3,700 $cm^{-1}$, which are typical absorption peaks of magnesia. The absorption peak at low frequencies near 440 $cm^{-1}$ was attributed to Mg-O [43]. This proved that $Mg(OH)_2$ precipitates were generated during the coagulation process.

FT-IR results showed that new chemical substances were formed during the coagulation process.

The XRD pattern of floc sediment when $MgCl_2$ was used as a coagulant is shown in Fig. 11(d). The comparison with the PDF standard card shows that $Mg(OH)_2$ existed in the precipitates of DO, DY and DB after coagulation with $MgCl_2$. This was consistent with the results of the FT-IR spectrum. However, the XRD pattern of the precipitate formed after the coagulation of $AlCl_3$ and $FeCl_3$ had no obvious characteristic peaks, which proved that the $AlCl_3$ and $FeCl_3$ produced in the solution were amorphous hydroxides, that is, amorphous precipitates.

4-3. The Effect of Coagulant Addition Order

The coagulant hydrolyzed instantaneously when it was put into an aqueous solution. The normal coagulation sequence is to add first the coagulant to the wastewater. In this experiment, the contribution of the instantaneous hydrolysate and the final hydrolysate of the coagulant to the color removal efficiency of dyes was investigated by changing the sequence of the coagulant addition (that is, adding the coagulant to the aqueous solution first to complete the hydrolysis, and then adding the dye to complete the coagulation process). Under the optimal dosage of coagulant, the effect of changing the order of adding coagulant and dye on color removal efficiency is shown in Fig. 12.

The results show that the order of coagulant dosing had no obvious effect on the color removal of $AlCl_3$ and $MgCl_2$. This indicates that the coagulation effect of $AlCl_3$ and $MgCl_2$ on direct dyes was mainly due to the final hydrolysate. From the FT-IR and XRD pattern analysis of flocs formed by the reaction of $AlCl_3$, $MgCl_2$ and direct dyes; the amorphous hydroxide produced by the hydrolysis of $AlCl_3$ chemically combined with the $-SO_3H$ in the direct dyes molecule, which allowed the direct dyes to be removed from the aqueous solution. The magnesium hydroxide precipitate formed by the hydrolysis of $MgCl_2$ chemically combined with the $-SO_3H$ of the direct dyes. Changing the order of adding $FeCl_3$ reduced the color removal of the three direct dyes, but the color removal still reached above 50%. This indicates that both the instantaneous hydrolysate and final hydrolysate of $FeCl_3$ in aqueous solution played an important role in the removal of direct dyes. After the coagulant was added to water, polyhydroxyl complex ions were formed and their hydroxyl groups were unsaturated. These complexes absorbed hydroxyl groups from the solution to supplement their unsaturated sites and formed strong adsorption on colloidal particles [44]. The amorphous hydroxide formed by the hydrolysis of

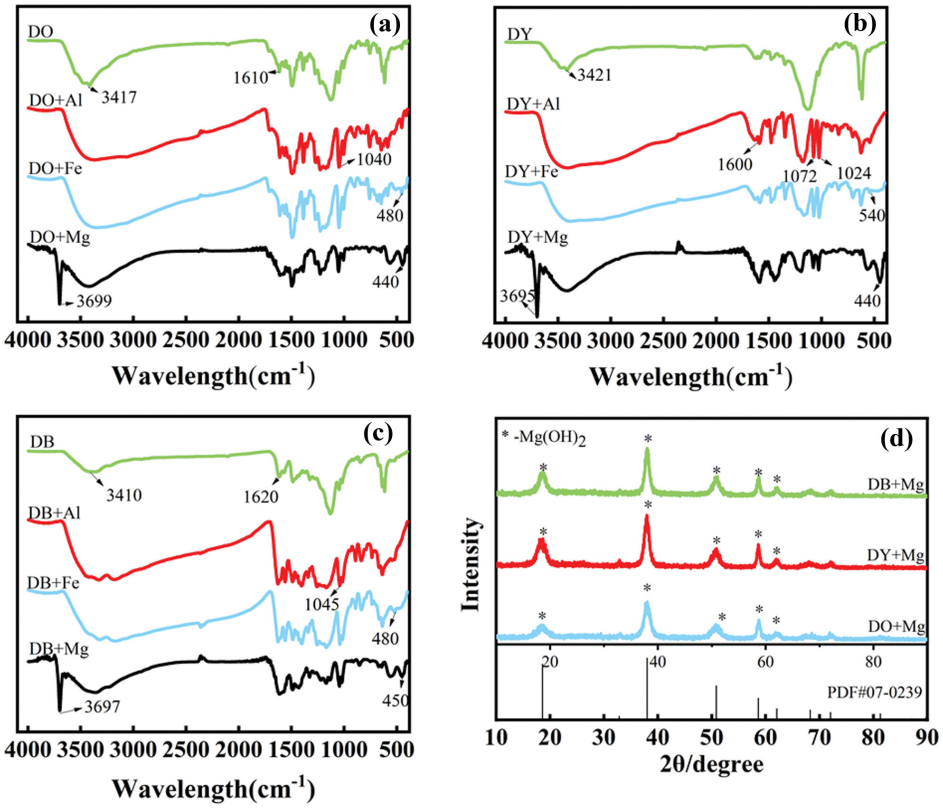



**Fig. 11. FT-IR spectra: (a) DO treated with $AlCl_3$, $FeCl_3$ and $MgCl_2$; (b) DY treated with $AlCl_3$, $FeCl_3$ and $MgCl_2$; (c) DB treated with $AlCl_3$, $FeCl_3$ and $MgCl_2$; and (d) XRD spectra of direct dyes treated with $MgCl_2$.**

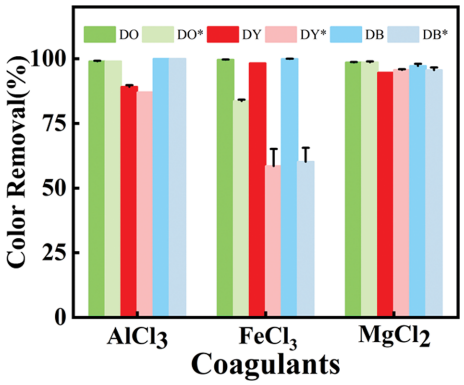



**Fig. 12. The effect of changing the dosing order of coagulant on color removal: No "*" means adding dyes first and then adding coagulant. "*" means adding coagulant first and then adding dye.**

$FeCl_3$ chemically combined with the direct dye to form particles with a certain particle size, so that the dye was removed from the aqueous solution.

In summary, the coagulation mechanism of $AlCl_3$, $FeCl_3$ and $MgCl_2$ is explained as shown in Fig. 13.

Charge neutralization was the basis for the formation of flocs. The monomer hydrolysates or poly-nuclear hydrolysates produced by the hydrolysis of the three coagulants in the water exerted a charge neutralization effect. These hydroxide species were deposited on the surface of the colloidal particles so that the colloidal particles began to destabilize and agglomerate. Generally, colloidal particles casrry negative charges and metal hydroxides carry positive charges. Therefore, in this process the Zeta potential approached from a negative value to zero and then the Zeta potential became positive, signifying that a charge reversal phenomenon occurred.

Chemical combination was the key to floc formation. The final hydrolysate of $AlCl_3$ played a major role in the removal of direct dyes. XRD pattern analysis showed that after $AlCl_3$ was hydrolyzed, amorphous hydroxide precipitates were formed and these hydroxide precipitates had a fairly open structure. The $-SO_3H$ on the direct dye molecule chemically combined with the hydroxide precipitate, so that the dye was adsorbed and wrapped in the growing hydroxide precipitate and removed quickly [32]. The instantaneous hydrolysate and the final hydrolysate of $FeCl_3$ played a combined role in the process of coagulation to remove direct dyes. The hydrolyzed product chemically combined with the $-SO_3H$ on the direct dye molecule to form flocs with a certain particle size, resulting in the removal of the direct dye from the aqueous solution.

Bridging and sweep flocculation processes were complementary in the floc removal. Macromolecular flocs further played the role of bridging and sweep flocculation during the sedimentation process to quickly and massively remove colloidal particles in the water.

## CONCLUSIONS

We selected three coagulants to explore their coagulation char-

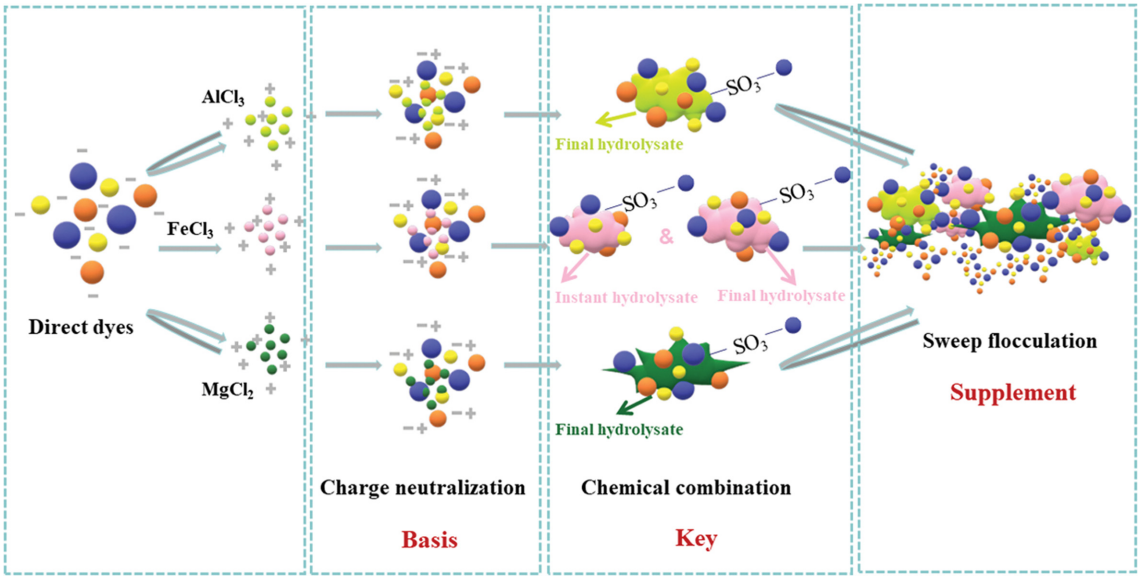



**Fig. 13. The coagulation mechanism diagram of direct dyes removed by$AlCl_3$, $FeCl_3$, $MgCl_2$.**

acteristics and mechanism on direct dyes. $AlCl_3$, $FeCl_3$ and $MgCl_2$ had a good coagulation effect on three direct dyes at low dosage of coagulant. The suitable pH range for $AlCl_3$ and $FeCl_3$ was 6-7, whereas that for $MgCl_2$ was 11-12. Choosing an appropriate rapid mixing time and slow stirring speed is beneficial in increasing the color removal and reducing the residual turbidity. The best rapid mixing time in this experiment was 30 or 60 s, while the best slow stirring speed was 50 r/min. The coagulation mechanism of $AlCl_3$, $FeCl_3$ and $MgCl_2$ on direct dyes was clarified, by further using FT-IR and XRD charge characteristic analysis and varying the level of coagulant dosing. This study showed that charge neutralization was the basis for floc formation, whereas chemical combination was the key to floc formation. Direct dyes were removed by the chemical combination of the hydrolysate of $AlCl_3$, $FeCl_3$ and $MgCl_2$ with the $-SO_3H$ on the direct dye molecule. The final hydrolysate of $AlCl_3$ and $MgCl_2$ played a major role, while both the instantaneous hydrolysate and the final hydrolysate of $FeCl_3$ played a role in the overall coagulation. At the same time, the combination mechanism of coagulant and dye was further clarified. The research results in this study will perfect and enrich the basic data of dye removal by coagulation. This study provides a practical guidance for selecting suitable coagulants to treat dye-containing wastewater, and at the same time provides basic data and theoretical support for the development of new coagulants.

## ACKNOWLEDGEMENTS

This work was supported by the National Natural Science Foundation of China (NSFC) (No. 21876025). This work was supported in part by the National Key Research and Development Program of China (Grant No. 2019YFC0408304).

## REFERENCES

1. S. Samsami, M. Mohamadi, M.-H. Sarrafzadeh, E. R. Rene and M. Firoozbahr, *Process Saf. Environ. Prot.*, **143**, 138 (2020).
2. J. Dotto, M. R. Fagundes-Klen, M. T. Veit, S. M. Palácio and R. Bergamasco, *J. Clean. Prod.*, **208**, 656 (2018).
3. H. Shah, K. Muhammad, K. S. Ali, S. Kausar, S. Zarbad, S. Hongli, K. Qadeer, S. A. Basit, R. W. Ur, A. G. Youssef O. and G. Usman, *Int. J. Biol. Macromol.*, **168**, 383 (2021).
4. D. Hailu, A. Guangyu, R. Y. Jiao, R. Tharindu, S. Lu and D. S. Wang, *Sep. Purif. Technol.*, **259**, 1 (2021).
5. V. Javanbakht and M. Mohammadian, *J. Mol. Struct.*, **1239**, 130496 (2021).
6. C. Peng, L. Chen, X. Wu, X. Wei, A. Tehrim, M. Dai and S. Xu, *J. Environ. Chem. Eng.*, **9**, 105690 (2021).
7. R. Wang, X. Jin, Z. Y. Wang, W. T. Gu, Z. C. Wei, Y. J. Huang, Z. Qiu and P. K. Jin, *Bioresour. Technol.*, **247**, 1233 (2018).
8. H. Zhao, R. Wang, H. Deng, L. Zhang, L. Gao, L. Zhang and T. Jiao, *ACS Omega*, **6**, 294 (2021).
9. R. Rehman, S. K. Lahiri, A. Islam, P. Wei and Y. Xu, *ACS Omega*, **6**, 22188 (2021).
10. N. C. L. Beluci, G. A. P. Mateus, C. S. Miyashiro, N. C. Homem, R. G. Gomes, M. R. Fagundes-Klen, R. Bergamasco and A. M. S. Vieira, *Sci. Total Environ.*, **664**, 222 (2019).
11. H. Eslami, A. Esmaeili, M. H. Ehrampoush, A. A. Ebrahimi, M. Taghavi and R. Khosravi, *J. Water. Process. Eng.*, **36**, 101342 (2020).
12. Y. Li, T. Zhang and H. Zhou, *Material Protection*, **52**, 104 (2019).
13. A. K. Badawi and K. Zaher, *J. Water. Process. Eng.*, **40**, 101963 (2021).
14. W. Tianzhi, W. Weijie, H. Hongying and S.-T. Khu, *J. Clean. Prod.*, **312**, 127798 (2021).
15. B. Shi, G. Li, D. Wang, C. Feng and H. Tang, *J. Hazard. Mater.*, **143**, 567 (2007).
16. E. F. Aboelfetoh, A. E. Aboubaraka and E. M. Ebeid, *J. Environ. Manage.*, **288**, 112481 (2021).
17. M. A. Ahangarnokolaei, B. Ayati and H. Ganjidoust, *Environ. Technol. Inno.*, **22**, 101459 (2021).
18. L. Kanhaiya and G. Anurag, *J. Environ. Chem. Eng.*, **7**, 1 (2019).

19. A. K. Tolkou, M. Mitrakas, I. A. Katsoyiannis, M. Ernst and A. I. Zouboulis, *Chemosphere*, **231**, 528 (2019).
20. Y. F. Wang, B. Y. Gao, Q. Y. Yue and Y. Wang, *J. Environ. Sci.*, **23**, 1626 (2011).
21. I. O. Adebayo, O. O. Olukowi, Z. Zhiyuan and Y. Zhang, *J. Water. Process. Eng.*, **44**, 102322 (2021).
22. R. Y. Jiao, R. Fabris, C. W. K. Chow, M. Drikas, J. v. Leeuwen, D. S. Wang and Z. Z. Xu, *J. Environ. Sci.*, **57**, 338 (2017).
23. S. Lu, L. Liu, Q. Yang, H. Demissie, R. Jiao, G. An and D. Wang, *Sci. Total Environ.*, **786**, 147508 (2021).
24. H. Demissie, G. An, R. Jiao, T. Ritigala, S. Lu and D. Wang, *Sep. Purif. Technol.*, **259**, 1 (2021).
25. K. L. Yeap, T. T. Teng, B. T. Poh, N. Morad and K. E. Lee, *Chem. Eng. J.*, **243**, 305 (2014).
26. Z. L. Yang, X. X. Liu, B. Y. Gao, S. Zhao, Y. Wang, Q. Y. Yue and Q. Li, *Sep. Purif. Technol.*, **118**, 583 (2013).
27. W. P. Li, J. F. Lu, M. L. Liu and J. H. Zhao, *Chem. Ind. Eng. Pro.* (China), **36**, 4286 (2017).
28. A. Z. Bouyakoub, B. S. Lartiges, R. Ouhib, S. Kacha, A. G. E. Samrani, J. Ghanbaja and O. Barres, *J. Hazard. Mater.*, **187**, 264 (2011).
29. W. Z. Yu, J. Gregory, L. Campos and G. B. Li, *Chem. Eng. J.*, **171**, 425 (2011).
30. P. Bubakova, M. Pivokonsky and P. Filip, *Powder. Technol.*, **235**, 540 (2013).
31. R. K. Chakraborti, K. H. Gardner, J. Kaur and J. F. Atkinson, *J. Water. Supply. Res. T.*, **56**, 1 (2007).
32. F. McYotto, Q. S. Wei, D. K. Macharia, M. H. Huang, C. S. Shen and C. W. K. Chow, *Chem. Eng. J.*, **405**, 126674 (2021).
33. S. Yang, W. Li, H. J. Zhang, Y. B. Wen and Y. H. Ni, *Sep. Purif. Technol.*, **209**, 238 (2018).
34. Y. Guo, L. Du, Q. Li and H. Xu, *Chinese. J. Chem. Eng.*, **10**, 1847 (2016).
35. B. Y. Gao, Q. Y. Yue and W. Yan, *J. Environ. Manage.*, **82**, 167 (2007).
36. K. Chinoune, K. Bentaleb, Z. Bouberka, A. Nadim and U. Maschke, *Appl. Clay. Sci.*, **123**, 64 (2016).
37. P. Juntunen, M. Liukkonen, M. Lehtola and Y. Hiltunen, *Cogent. Eng.*, **1**, 3969 (2014).
38. Q. Meng, J. Nan, Y. B. Gong and M. Q. Guo, *Water Wastewater Eng.*, **56**, 88 (2020).
39. L. Tang, F. Xiao, Q. Wei, Y. Liu, Y. Zou, J. Liu, W. Sand and C. Chow, *Chemosphere*, **223**, 204 (2019).
40. L. G. Liu, C. D. Wu, Y. C. Chen and H. P. Wang, *Water Sci. Technol.*, **75**, 137 (2017).
41. A. Al-Mashaqbeh, B. El-Eswed, R. Banat and F. I. Khalili, *Environ. Nanotechnol., Monit. Manage.*, **10**, 351 (2018).
42. J. W. Liu, S. H. Cheng, N. Cao, C. X. Geng, C. He, Q. Shi, C. M. Xu, J. R. Ni, R. M. DuChanois, M. Elimelech and H. Zhao, *Nat. Nanotechhnol.*, **14**, 64 (2019).
43. Y. X. Wei, A. M. Ding, L. Dong, Y. Q. Tang, F. L. Yu and X. Z. Dong, *Colloids Surf. Physicochem. Eng. Aspects*, **470**, 137 (2015).
44. Y. N. L. B. L. Li, C. C. Zhang, Y. Yao, W. Q. Zhang and Y. Li, *Acta. Sci. Circum*, **36**, 2503 (2016).